Short Title: Physiological traits of *Rhazya stricta* associated with optimal photosynthetic performance under elevated temperature

Corresponding Author: Berkley J. Walker
Email: berkley@msu.edu
Phone: (517) 355-3928

Title: Increased activity of core photorespiratory enzymes and CO_2 transfer conductances are associated with higher and more optimal photosynthetic rates under elevated temperatures in the extremophile *Rhazya stricta*

Complete Author List

Luke M. Gregory[1,2]
grego215@msu.edu

Ludmila V. Roze[1]
roze@msu.edu

Berkley J. Walker[1,2]
berkley@msu.edu

[1] Department of Energy-Plant Research Laboratory, Michigan State University, East Lansing, MI 48824, USA
[2] Department of Plant Biology, Michigan State University, East Lansing, MI 48824, USA

One Sentence Summary:

Increased activity of two core photorespiratory enzymes and adapted CO_2 transfer (stomatal and mesophyll) conductance was associated with more optimal photosynthetic performance under elevated temperatures in the C_3 extremophile *Rhazya stricta*.

List of Author Contributions:

BJW conceived the original research plans and supervised the research with input from LMG. and LVR. LVR performed the enzymatic activity assays, while LMG carried out the in-depth gas-exchange experiments. LMG analyzed the results and wrote the paper with contributions from all authors. BJW serves as the author responsible for contact.

Funding Information:

LMG, LVR and BJW were funded by the Division of Chemical Sciences, Geosciences, and Biosciences, Office of Basic Energy Sciences of the United States Department of Energy (DE-FG02-91ER20021), and National Science Foundation awards from the Division of Integrative Organismal Systems (2030337).

Abstract

Increased photorespiration and optimizing intrinsic water use efficiency are unique challenges to photosynthetic carbon fixation at elevated temperatures. To determine how plants can adapt to facilitate high rates of photorespiration at elevated temperatures while also maintaining water-use efficiency, we performed in-depth gas exchange and biochemical assays of the C_3 extremophile, *Rhazya stricta*. These results demonstrate that *R. stricta* supports higher rates of photorespiration under elevated temperatures and that these higher rates of photorespiration correlate with increased activity of key photorespiratory enzymes; phosphoglycolate phosphatase and catalase. The increased photorespiratory enzyme activities may increase the overall capacity of photorespiration by reducing enzymatic bottlenecks and allowing minimal inhibitor accumulation under high photorespiratory rates. Additionally, we found the CO_2 transfer conductances (stomatal and mesophyll) are re-allocated to increase the water-use efficiency in *R. stricta* but not necessarily the photosynthetic response to temperature. These results suggest important adaptive strategies in *R. stricta* that maintain photosynthetic rates under elevated temperatures with optimal water loss. The strategies found in *R. stricta* may inform breeding and engineering efforts in other C_3 species to improve photosynthetic efficiency at high temperatures.

Keywords: Photorespiration, *Rhazya stricta*, phosphoglycolate phosphatase, catalase, water-use efficiency, CO_2 transfer conductance

Table 1. Parameter definitions

Parameter	***Biological Description***	***Unit***
A	Net CO_2 assimilation rate	μmol m^{-2} s^{-1}
C_a	The CO_2 partial pressure in the ambient air	Pa
C_i	The CO_2 partial pressure in the intercellular airspace of the leaf	Pa
C_i^*	The CO_2 partial pressure in the intercellular airspace of the leaf at the photorespiratory compensation point	Pa
C_c	The CO_2 partial pressure in the chloroplast	Pa
g_{sw}	Stomatal conductance to H_2O in air	mol m^{-2} s^{-1}
g_{tc}	Stomatal conductance to CO2 in air	mol m^{-2} s^{-1}
g_m	Mesophyll conductance to CO_2	μmol m^{-2} s^{-1} Pa^{-1}
J_{max}	Maximum rate of electron transport	μmol m^{-2} s^{-1}
Lg_{tc}	Limitation imposed by stomatal conductance on net CO_2 assimilation rate	%
Lg_m	Limitation imposed by mesophyll conductance on net CO_2 assimilation rate	%
$S_{c/o}$	specificity of rubisco for CO_2 relative to O_2	unitless
R_L	Non-photorespiratory CO_2 release in the light	μmol m^{-2} s^{-1}
v_c	The velocity of rubisco carboxylation	μmol m^{-2} s^{-1}
$v_{c,max}$	The maximum velocity of rubisco carboxylation	μmol m^{-2} s^{-1}
v_o	The velocity of rubisco oxygenation	μmol m^{-2} s^{-1}
v_o/v_c	The velocity of rubisco oxygenation per carboxylation	unitless
Γ^*	The CO_2 partial pressure in the chloroplast at the photorespiratory compensation point	Pa
α	Stoichiometric release of CO_2 per oxygenation reaction	mol mol^{-1}
Δ_f	Discrimination associated with photorespiration	‰
f	$^{12}C/^{13}C$ fractionation during photorespiration	‰
Φ_{CO2}	Maximum quantum yield of CO_2 fixed per photon absorbed	unitless

121 ## *Introduction*

122 Global warming has increased the frequency of high temperature events that place
123 physiological constraints on C_3 photosynthetic performance. This warming is happening rapidly;
124 the most recent IPCC report estimates global surface temperatures will increase by 1.4°C –
125 4.8°C in the next century, meaning that future plants will experience higher temperatures than
126 they have experienced in at least the last 100,000 years (Pörtner *et al.*, 2022). Increasing global
127 surface temperatures will raise air temperature and alter atmospheric vapor pressure deficit
128 (VPD), which directly influences various physiological processes in plants (Moore *et al.*, 2021).
129 These physiological processes include enzymatic temperature response, leaf energy balance,
130 stomatal behavior, cell membrane properties, and changes in photosynthetic performance
131 (Larkindale *et al.*, 2004; Marcum, 1998; Moore *et al.*, 2021; Prasertthai *et al.*, 2022; Urban *et al.*,
132 2017a; Urban *et al.*, 2017b). While all these physiological processes are important,
133 photosynthetic performance under future climates is of particular interest due to its
134 participation in the global carbon cycle and recent efforts to improve its efficiency (De Souza *et*
135 *al.*, 2022; Kromdijk *et al.*, 2016; South *et al.*, 2018). Photorespiration and intrinsic water use
136 efficiency (*WUE*) will disproportionately affect C_3 species as temperatures increase since they
137 lack the carbon concentrating mechanism of C_4 or CAM species. Understanding how C_3 species
138 will manage higher photorespiratory fluxes and optimize *WUE* at elevated temperatures will
139 help us resolve temperature-dependent mechanisms and likely advance breeding and
140 engineering strategies in C_3 species.

141 Increased photorespiration limits C_3 photosynthetic performance at elevated temperatures.
142 The photorespiration pathway begins when O_2 binds to ribulose-1,5-bisphosphate
143 carboxylase/oxygenase (rubisco) instead of CO_2. The resulting oxygenation of ribulose-1,5-
144 bisphosphate (RuBP) produces 3-phosphoglycerate (3-PGA), a C_3 cycle intermediate, and 2-
145 phosphoglycolate (2-PG), an intermediate that inhibits the C_3 cycle enzymes triose phosphate
146 isomerase and sedoheptulose-1,7-bisphosphatase (Anderson, 1971; Flügel *et al.*, 2017). To
147 reduce the inhibition of the C_3 cycle enzymes, photorespiration detoxifies and recycles 2-PG
148 back into 3-PGA through a set of reactions that occur in the chloroplast, peroxisome,
149 mitochondrion, and cytosol (see Box 1). Although the photorespiratory pathway is an effective

150 solution to handle RuBP oxygenation, it lowers the efficiency of photosynthesis by reducing net
151 carbon fixation by releasing CO_2 (Bauwe *et al.*, 2012). Relative rates of RuBP oxygenation
152 increase with temperature due to decreases in rubisco specificity and decreased solubility of
153 CO_2 relative to O_2 (Hall *et al.*, 1983; Hermida-Carrera *et al.*, 2016; Jordan *et al.*, 1984).
154 Therefore, under elevated temperature, greater oxygenation rates will increase rates of 2-PG
155 production that need to be detoxified and recycled by the photorespiratory pathway.
156 While rubisco kinetics and gas solubilities determine the rate at which 2-PG is initially
157 produced following rubisco oxygenation, the temperature response of downstream
158 photorespiration and the effects on subsequent CO_2 loss is unclear. Loss of CO_2 occurs through
159 the decarboxylation of glycine in the mitochondrion; however, there is evidence for additional
160 release of CO_2 from non-enzymatic decarboxylation reactions that occur within the peroxisome,
161 especially under elevated temperatures (Abadie *et al.*, 2016; Bao *et al.*, 2021; Somerville, 2001;
162 Somerville *et al.*, 1980; Walker *et al.*, 2013). The CO_2 released from nonenzymatic
163 decarboxylation reactions combined with CO_2 loss from GDC would reduce net carbon fixation.
164
165
166
167
168
169
170
171
172
173
174
175
176
177
178

179 **BOX 1**

180

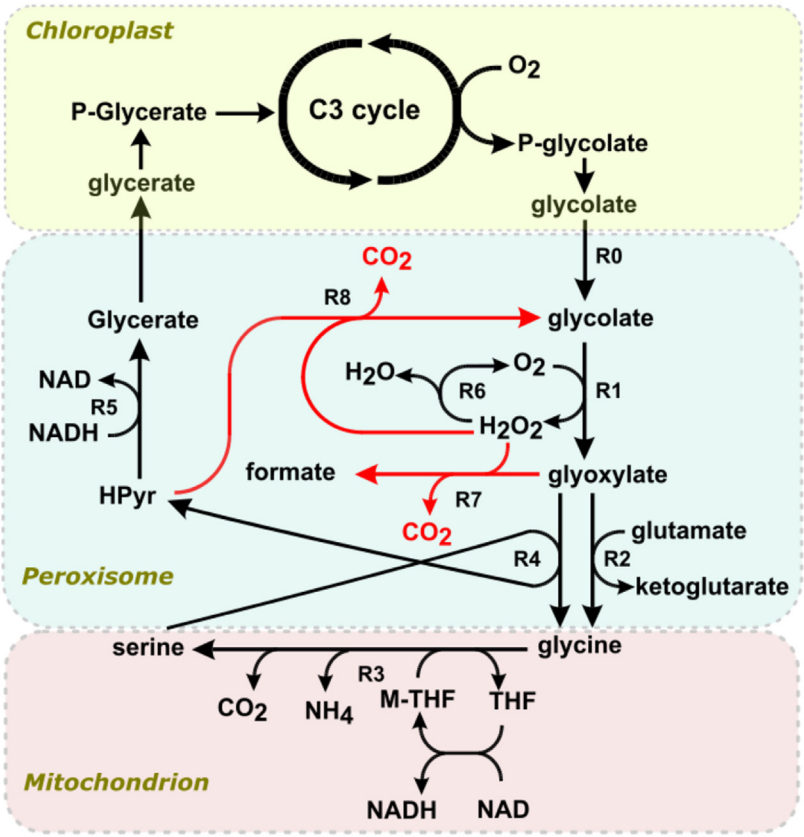

181 Following the oxygenation of RuBP by rubisco in the chloroplast, phosphoglycolate
182 phosphatase (PGP) converts 2-PG into glyoxylate. Glycolate in transported to the peroxisome
183 where glycolate oxidase (GO) catalyzes the conversion of glycolate and O_2 to glyoxylate and
184 hydrogen peroxide (H_2O_2). H_2O_2 is decomposed in the peroxisome into H_2O and O_2 by catalase
185 (CAT), while glyoxylate is animated with glutamate or alanine to produce glycine via
186 aminotransferase (GGAT or AGAT). Glycine in transported into the mitochondrion and
187 decarboxylated to produce serine by glycine decarboxylate complex and serine
188 hydromethyltransferase. Serine is transported back to the peroxisome and converted to
189 hydroxypyruvate by serine glyoxylate aminotransferase (SGAT). hydroxypyruvate is reduced by
190 hydroxypyruvate reductase (HPR) to form glycerate. Glycerate is transported back to the
191 chloroplast and catalyzed by glycerate kinase (GLYK) to 3-PGA, which re-enter the C_3 cycle.
192 Image reproduced from: Catalase protects against nonenzymatic decarboxylations during
193 photorespiration in *Arabidopsis thaliana*, Bao *et al.*, Plant Direct Volume 5 Issue 12. Copyright
194 (c) [2021] authors hold copyright and have given permission to reproduce.

208 Another challenge to maintaining C_3 photosynthetic performance at elevated temperatures
209 is preserving plant water. The driving force of water vapor loss or transpiration from the plant
210 to the atmosphere is VPD. VPD, which is the difference in water vapor partial pressure between
211 the intercellular airspace of the leaf and the atmosphere, responds to air temperature. As
212 temperatures rise, VPD increases curvilinearly and drives greater transpiration rates (Lawrence,
213 2005). The greater rates of transpiration alter CO_2 and H_2O exchange between plants and the
214 atmosphere and cause a greater water loss per carbon assimilated (or reduction in *WUE*)
215 because CO_2 and H_2O exchange through the same stomatal pore (Rawson *et al.*, 1977). While
216 the stomatal conductance (g_{sw}) constrains CO_2 and H_2O exchange with the atmosphere and the
217 intercellular airspace, mesophyll conductance (g_m) constrains only the transfer of CO_2 from the
218 intercellular airspace to the site of carboxylation without a corresponding loss of H_2O. Given the
219 ability of g_m to facilitate CO_2 transfer without accompanying H_2O loss, it is unclear to what
220 degree plants adapted to high temperatures have exploited this property to limit water loss
221 while maximizing CO_2 availability. The reduction of CO_2 availability through regulated decreases
222 in g_{sw} is large enough to decrease photosynthetic performance in C_3 plants, which lack a carbon
223 concentrating mechanism.
224 Does C_3 photosynthetic performance always decrease with increasing temperatures, or
225 have some C_3 species adapted to facilitate high rates of photorespiration while maintaining
226 photosynthesis and *WUE* at elevated temperatures? To explore this question, we investigated
227 how *Rhazya stricta*, a C_3 desert extremophile, has adapted to maintain photosynthetic
228 performance at elevated temperatures. *R. stricta* is ideal for studying heat adaptation as it is
229 native to hot-arid environments. Past work suggests that *R. stricta* has distinct physiological
230 adaptations to extreme temperatures (Lawson et al., 2014; Yates et al., 2014). For example, leaf
231 temperature during *in situ* diurnal measurements of *R. stricta* climbed from 26°C to 43°C with
232 an accompanying increase in photorespiration (Lawson *et al.*, 2014). During this increase in
233 temperature, the relative water content in the leaf was stable, suggesting there was minimal
234 water stress.
235 In this paper, we determine how *R. stricta* facilitates high rates of photorespiration while
236 maintaining photosynthesis and *WUE* at elevated temperatures. Here, we hypothesize that *R.*

stricta maintains photorespiratory capacity at elevated temperatures through increased activity of key photorespiratory enzymes. We additionally hypothesize that *R. stricta* optimizes *WUE* by favoring g_m relative to g_{sw} under elevated temperatures. To test these hypotheses, we compared various physiological and biochemical parameters in two species, *Nicotiana tabacum*, a thermotolerant C_3 species, and *R. stricta*, an extremophilic C_3 species. The results from these measurements indicate that *R. stricta* maintains higher rates of photorespiration than *N. tabacum* under moderate and elevated temperatures and that these higher rates of photorespiration correlate with increased activity of key photorespiratory enzymes; phosphoglycolate phosphatase and catalase. Additionally, the g_{sw} and g_m appear to be optimized for water-use efficiency but not necessarily photosynthetic carbon gain to temperature in *R. stricta*. These results suggest important adaptive strategies in *R. stricta* that maintain photosynthetic rates under elevated temperatures with optimal water loss.

266 ## *Material and Methods*

267 **Plant Material and Growth Conditions**

268 *R. stricta* seeds were wild collected for this study and are available through the
269 Millennial Seed Bank coordinated by the Royal Botanical Gardens, Kew Serial number 220547.
270 Prior to planting, *R. stricta* seeds were surface-sterilized inside a Laminar hood with 100%
271 ethanol for five minutes followed by a seven-minute soak in 25% bleach solution. Seeds were
272 then washed and vortexed three times in deionized water. After sterilization, seeds germinated
273 in a petri dish filled with deionized water for two-weeks. During the two weeks, water was
274 changed as needed to remove yellow exudate to avoid possible allelopathic inhibition of
275 germination. Seeds were transferred when roots emerged and were 1 cm in length to 11.36 L
276 pots containing half Sure-Mix potting soil (Michigan Grower Products, Inc., Galesburg, MI) and
277 half sand mixture. *R. stricta* were grown for an additional eight weeks until leaves were large
278 enough for gas exchange measurements. *N. tabacum* were sown and grown in 0.7 L pots
279 containing Sure-Mix potting soil (Michigan Grower Products, Inc., Galesburg, MI) for 4-6 weeks
280 until leaves were large enough for gas exchange measurements. Both *R. stricta* and *N. tabacum*
281 plants were grown in a greenhouse with an average day/night temperature of 34/27 °C and a
282 16/8 photoperiod of supplemental light (150 µmol m^{-2} s^{-1}). Plants were watered as needed with
283 ½-strength Hoagland's solution.

284

285 **Estimating C_i* and R_L using the common intersection method**

286 Gas exchange was measured on the youngest, fully expanded leaves of *R. stricta* and
287 *N. tabacum* using a LI-6800 (LI-COR Biosciences, USA) using a 9 cm^2 chamber with 50:50
288 blue:red LEDs to better replicate the blue to red ratio of the solar spectrum at the earth's
289 surface. To shift between temperatures ranging from 20°C to 40°C, the LI-6800 was placed
290 inside a climate-controlled chamber (Percival Scientific, USA). The apparent CO_2 compensation
291 point uncorrected for g_m (C_i*) and rates of CO_2 release from non-photorespiratory processes in
292 the light (R_L) were measured using the common intersection method (Laisk, 1977; Walker *et al.*,
293 2016a). During the measurement, steady-state *A* was measured at 3, 5, 7, 9, 11, 40 pascal (Pa)
294 CO_2 under various light intensities (250, 165, 120, 80, 50 µmol PAR m^{-2} s^{-1}), with a flow rate of

295 500 µmol s^{-1}. Linear fits of the CO_2 response curves were made for each light intensity. A linear
296 regression of the slope-intercept from these linear fits was used to estimate C_i* and R_L.
297
298 **Measuring g_m with gas exchange and ^{13}C isotope discrimination**
299 g_m was measured using *in vivo* gas exchange combined with on-line measurements of
300 the carbon isotope discrimination method with our particular system as described previously
301 (Fu *et al.*, 2023). Briefly, gas exchange was performed as above using an LI-6800 with 9 cm^2
302 chamber with 50:50 blue:red LEDs. To measure carbon isotope discrimination, the LI-6800 was
303 coupled to a tunable infrared laser differential absorption spectrometer (TILDAS-CS, Aerodyne
304 Research, USA). The CO_2 in the leaf chamber, flow rate, and irradiance were set to 40 Pa CO_2,
305 300 µmol s^{-1}, 1750 µmol PAR m^{-2} s^{-1}, respectively. Measurements were made under 2% O_2 to
306 minimize uncertainties about precise photorespiratory fractionation (*f*) values and since g_m has
307 not been shown to be oxygen dependent (further validated below). To measure under 2% O_2,
308 N_2 and O_2 were mixed by mass-flow controllers (Alicat Scientific, Inc., USA). For calibrating the
309 $\delta^{13}C$ values, a reference line was supplied with isotopically characterized CO_2 ($\delta^{13}C$ vs. VPDB: -
310 4.6 ± 0.3 ‰, (Airgas Specialty Gases, USA)). Leaves were measured after reaching steady-state
311 assimilation rate (*A*) at each temperature starting at 20°C and increasing to 40°C, by 5°C steps.
312 g_m was calculated from carbon isotope equations presented previously (Ubierna *et al.*, 2018)
313 that build upon foundation work in isotope-ration mass spectroscopy-based approaches in
314 isotope discrimination (Evans *et al.*, 1986; Farquhar *et al.*, 1982; Farquhar *et al.*, 2012) and the
315 recent advances in online methods using tunable diode lasers (Barbour *et al.*, 2007; Tazoe *et al.*,
316 2011; von Caemmerer *et al.*, 2015).
317
318 **Measuring the temperature response for photorespiratory discrimination and fractionation**
319 Photorespiratory discrimination (Δ_f) and the $^{12}C/^{13}C$ fractionation during
320 photorespiration (*f*) for *R. stricta* and *N. tabacum* were resolved using the *in vivo* gas exchange
321 combined with on-line measurements of the carbon isotope discrimination (described above).
322 Leaves were measured at 25°C and 35°C, both at 2% and 21% oxygen. g_m was determined at 2%
323 oxygen where photorespiratory release of CO_2 was minimized assuming f = 11.8‰ (with the

corresponding rubisco ^{13}C fractionation; 30‰) (Tcherkez, 2006; Ubierna *et al.*, 2018). We then assumed the g_m measurements at 2% oxygen were the same as the g_m at 21% oxygen to solve for Δ_{gm} at both measuring temperatures. g_m was also determined assuming f = 11.8‰ for both oxygen concentrations for each temperature. We could calculate Δ_f using:

$$\Delta_f = \Delta_i - \Delta_o - \Delta_{g_m} - \Delta_e \tag{1}$$

Then, with Δ_f, derive f by:

$$f = \frac{1-t}{1+t}\frac{\alpha_e}{\alpha_f}\Delta_f\frac{C_a}{A} \tag{2}$$

(Evans *et al.*, 2013; Ubierna *et al.*, 2018)

Calculating *Γ***

*Γ** in *R. stricta* and *N. tabacum* was calculated using C_i*, R_L and g_m. *Γ** was determined according to

$$\Gamma^* = C_i^* + \frac{R_L}{g_m} \tag{3}$$

(Von Caemmerer, 2000). To account for internal dependency on solved parameters, g_m and *Γ** were re-solved iteratively using previous g_m, and *Γ** values; iterations continued until there was negligible change in re-solved g_m, and *Γ**.

Estimating rates of v_c and v_o

v_c and v_o for *R. stricta* and *N. tabacum* were estimated according to

$$v_c = \frac{A + R_L}{1 - \Gamma^*/C_c} \tag{4}$$

$$v_o = \frac{v_c - A - R_L}{0.5} \quad (5)$$

346 (Walker *et al.*, 2020). Where, the partial pressure of CO_2 at the site of rubisco catalysis (C_c) was
347 determined by

$$C_c = C_i - \frac{A}{g_m}. \quad (6)$$

348

349 **Finding saturating light intensity and maximum quantum yield**

350 Gas exchange was measured on the youngest, fully expanded leaves of *R. stricta* and
351 *N. tabacum* using a LI-6800 (LI-COR Biosciences, USA) using a 6 cm^2 chamber with 50:50
352 blue:red LEDs. During the measurement, steady-state *A* was measured at 40 Pa CO_2 under
353 monotonically decreasing light intensities (2000, 1500, 1000, 750, 500, 350, 250, 150, 75, 50,
354 45, 40, 35, 30, 25, 20, 15, 10, 5 µmol PAR m^{-2} s^{-1}) with a flow rate of 500 µmol s^{-1}. The leaf
355 absorptivity in R. stricta and N. tabacum leaves was measured using a SpectroClip-JAZ-TR
356 integrating sphere (Ocean Optics inc., USA) and used to calculate absorbed quanta. To find
357 maximum quantum yield of CO_2 fixed per photon absorbed, the relationship of assimilation to
358 absorbed quanta was then fit to a linear regression at low light intensity.

359

360 **Measuring $v_{c,max}$ and J_{max} with the Dynamic Assimilation Technique**

361 Gas exchange was measured on the youngest, fully-expanded leaves of *R. stricta* and
362 *N. tabacum* using a LI-6800 (LI-COR Biosciences, USA) with a 6 cm^2 chamber with 50:50 blue:red
363 LEDs. To shift between temperatures ranging from 20°C to 40°C, the LI-6800 was located inside
364 of a climate-controlled chamber (Percival Scientific, USA). Range matching and dynamic
365 calculations were preformed according to manufacturer's instructions. CO_2 response curves for
366 fitting maximum rate of rubisco carboxylation ($v_{c,max}$) and maximum rate of electron transport
367 (J_{max}) were measured under saturating light (1750 µmol PAR m^{-2} s^{-1}) from 150 Pa CO_2 to 5 Pa
368 CO_2 with a flow rate of 200 µmol s^{-1}. Leaves stabilized at 150 Pa CO_2 at the measuring
369 temperature for 30-40 minutes before decreasing CO_2 concentrations monotonically. This
370 method was utilized to reduce the oscillations that occur under triose-phosphate utilization
371 limitation (McClain *et al.*, 2023); however, this parameter could still not properly be fitted. $v_{c,max}$

and J_{max} were estimated using an R-based *ACi* fitting tool (Gregory *et al.*, 2021) (see https://github.com/poales/msuRACiFit to access Rscript with user-friendly interface).

We used the Dynamic Assimilation Technique rather than using a steady-state method to generate the CO_2 response curves to facilitate measuring enough multiple temperatures in a reasonable amount of time. Response curves that utilize continuous ramping of CO_2 began with the Rapid A-C_i Response (RACiR) technique (Stinziano *et al.*, 2017) paving the way for a more robust method (relative to the RACiR approach) based on re-deriving the equations for gas exchange for the non-steady state and implementing a range match to account for slight calibration differences between the sample and reference infra-red gas analyzers (Saathoff *et al.*, 2021). The speed in which the CO_2 response curves can be obtained (i.e., 5-7 minutes) compared to the traditional (i.e., 40-45 minutes) was especially important for measuring each genotype under a range of temperatures where we wanted to limit the plant's exposure to each condition.

Calculating Lg_{tc}, Lg_m and WUE

Using the CO_2 response curves from above, Lg_{tc} and Lg_m were calculated at ambient CO_2 concentration (40-42 Pa CO_2). Lg_{tc} was calculated according to

$$L_{g_{tc}} = \frac{A_{sl} - A_n}{A_{sl}} \quad (7)$$

(Warren, 2004). Where A_n is the A that occurs at C_a 40-42 Pa CO_2 and A_{sl} (assuming no stomatal resistance) is the A that occurs when C_i 40-42 Pa CO_2. Lg_{tc} was calculated according to

$$L_{g_m} = \frac{A_{ml} - A_n}{A_{ml}} \quad (8)$$

where A_{ml} (assuming stomatal but no mesophyll resistance) is the A that occurs when $C_c = C_i$ when C_a is 40-42 Pa CO_2. *WUE* was calculated from gas exchange measurements at 40 Pa CO_2 according to

$$WUE = \frac{A}{g_{sw}} \quad (9)$$

399 (Vialet-Chabrand *et al.*, 2016).

400

401 **Preparing crude protein extract for protein quantification and enzymatic assays**

402 Crude protein extracts were prepared from the youngest, fully expanded leaves of *R.*
403 *stricta* and *N. tabacum*. Leaf punches were removed from *R. stricta* and *N. tabacum* using a
404 cork borer (8.15 mm and 17 mm), immediately frozen in liquid N_2, and stored at -80°C. Leaf
405 material was homogenize on ice with 1 mL of the Extraction buffer (50 mM EPPS buffer, pH 8.0,
406 containing 1 mM EDTA, 10 mM DTT, 0.1% Triton X-100 [v/v], 0.5% polyvinylpyrrolidone, and 10
407 uL 1X SigmaFAST Protease Inhibitor Cocktail, EDTA Free (Sigma, St. Louis, MO, USA)), using a 2
408 mL glass-to-glass homogenizer (Kontes Glass Co., Vineland, NJ, USA). The homogenate was
409 transferred into a 1.5 mL plastic Eppendorf tube and clarified by centrifugation for 10 min at
410 13,500 g and 4◦C (Eppendorf Centrifuge 5424R). The supernatant, containing the clarified crude
411 protein extract, was used for protein quantification and enzyme assays.

412

413 **Protein quantification**

414 Soluble protein content was determined in crude protein extract (Bio-Rad Protein Assay;
415 BIO-RAD, USA) according to the manufacturer instructions using a SpectraMax M2 Microplate
416 Reader (Molecular Devices, San Jose, CA, USA).

417

418 **Enzymatic Assays**

419 All enzyme activities were measured by spectrophotometric assays with the use of
420 SpectraMax M2 Plate reader and SoftMax Pro7 software (Molecular Devices, San Jose, CA,
421 USA). PGP, GO, GGAT, AGAT, SGAT, HPR, and GLYK assays were performed in a 200 µL total
422 reaction mix using polystyrene or acrylic UV transparent 96-well microplates (Corning,
423 Kennebunk, ME, USA), while the CAT assay was performed in 1 mL reaction mix using a quartz
424 cuvette. The pH of reactions was selected based on the organellar pH where the reaction occurs
425 (Heinze *et al.*, 2002; Kendziorek *et al.*, 2008; Liu *et al.*, 2008; Shen *et al.*, 2013). All enzyme
426 assays were performed across two temperatures (25 °C and 35°C) with three technical

427 replicates. There were 4 – 5 independent biological replicates measured using leaf tissue from
428 different plants.
429
430 **Phosphoglycolate phosphatase (PGP) activity**
431 PGP activity was determined in *R. stricta* and *N. tabacum* colormetrically by the
432 production of inorganic phosphate with the following modifications (Pai *et al.*, 1990; Schwarte
433 *et al.*, 2007). 194 µL of reaction buffer (50 mM HEPES buffer, pH 7.5, 1 mM EDTA, and 10 mM
434 $MgCl_2$) were combined with 4 µL of crude protein extract and 2 µL 200 mM 2-PG was added to
435 initiate the reaction. The addition of the substrate was performed using a 96-well microplate
436 replicator (Boekel, Feasterville-Trevose, PA, USA). After 5 min the reaction was terminated by
437 addition 32 µL of Pi reagent (2.5 N H_2SO_4, 0.2 mM antimony potassium tartrate, 4.9 mM
438 ammonium molybdate, and 30 mM ascorbic acid). The plate was covered with parafilm, and the
439 spectrophotometric readings were taken after 45 min at 880 µm using SpectraMax M2. To
440 adjust for Pi that was produced independently from the PGP reaction, a control, containing
441 reaction buffer and crude protein extract, was incubated for 5 min, then the reagent was added
442 followed by 2-PG. A standard curve for Pi was constructed in the range 0.05 – 0.35 ug Pi per
443 well using KH_2PO_4. PGP specific activity was expressed in µmoles of 2-phosphoglycolate m^{-2} s^{-1}.
444
445 **Glycolate oxidase (GO) activity**
446 The activity of GO was determined in *R. stricta* and *N. tabacum* by formation of
447 glyoxylate phenylhydrazone (Baker *et al.*, 1966; Zelitch *et al.*, 2008) with the following
448 modifications. The reaction mix contained 20 µL 0.5 mM K-phosphate buffer, pH 8.1, 10 µL of
449 110 mM phenylhydrazine, 10 µL 1.3 mM riboflavin, 3 µL crude protein extract, 152 µL sterile nQ
450 water and 5 µL of 100 mM glycolic acid. The reaction was initiated with glycolic acid after the
451 mix was pre-incubated for 5 min without the substrate. The addition of the substrate was
452 performed with the use of a 96-well microplate replicator (Boekel, Feasterville-Trevose, PA,
453 USA). Control contained 5 µL water instead of the substrate. The increase in OD at 324 um was
454 measured in an acrylic UV transparent plate (Corning, Kennebunk, ME, USA) for 5 min every 10

455 sec. GO specific activity was calculated using the molar extinction coefficient of the glyoxylate-
456 phenylhydrazone complex (17 mM^{-1} cm^{-1}) and expressed as µmol glyoxylate m^{-2} s^{-1}.
457
458 **Catalase (CAT) activity**
459 The activity of CAT was determined in *R. stricta* and *N. tabacum* by the decomposition
460 of H_2O_2 (Aebi, 1983; Zelitch, 1989) with the following modifications. Small molecules from
461 crude protein extract from both species were excluded using a Spin-X UF 500 10 K MWCO
462 (Corning/Sigma-Aldrich, Inc. St. Louis, MO, USA) protein concentrator cartridges to removes low
463 molecular weight compounds, including specialized metabolites, which extensively absorb at
464 240 nm and interfere with the catalase assay. In brief, 300 µL crude protein extract and 200 µL
465 extraction buffer with no PVDP were applied to the concentrator cartridge and centrifuged for
466 25 min, 15,000 rcf, 4°C. After centrifugation, an additional 200 µL of extraction buffer with no
467 PVDP was added following another centrifugation under the same parameters. The extract
468 from the concentrator cartridge was adjusted to 300 µL with extraction buffer with no PVDP
469 before enzymatic assay so that catalase was not concentrated during this step. Since the
470 concentrator membrane removes molecules up to 10 kDa and the molecular weight of catalase
471 is ~60 kDa, catalase was not lost during this step and was not likely diluted or concentrated on a
472 volume (or by extension, an area) basis. It is possible that soluble proteins lower than 10 kDa
473 passed through the concentrator, resulting in an increase in catalase activities expressed on a
474 protein basis. This protein loss was ~10% of the total soluble protein as determined by a
475 Bradford assay.
476 The reaction mix containing 965.5 µL 50 mM K-phosphate buffer, pH 8.1, and 15 µL
477 extract, was incubated for 1.5 min to determine the rate of background change in optical
478 density. The reaction was initiated with 33.5 µL 30 mM H_2O_2 and the decline in optical density
479 at 240 nm was observed for 1.5 min with 10 sec intervals using spectrophotometer SpectraMax
480 M2. The initial rate of reaction was determined during first 30 sec and the specific activity was
481 expressed as µmoles H_2O_2 m^{-2} s^{-1} using molar extinction coefficient for H_2O_2 at 240 nm 43.6 M^{-}
482 $^{1}cm^{-1}$.
483

484 **Glutamate glyoxylate aminotransferase (GGAT), alanine glyoxylate aminotransferase (AGAT),**
485 **and serine glyoxylate aminotransferase (SGAT) activities**
486 The activity of GGAT, AGAT, and SGAT were determined spectrophotometrically as
487 described previously(Liepman *et al.*, 2001, 2003). Recombinant N-terminal 6xHis tagged HPR1
488 from *A. thaliana* was used as a coupling enzyme in the assay for SGAT. HPR1 was produced in *E.*
489 *coli* LMG194 using a plasmid pBADAtHPR1 (obtained from S. Timm, University of Rostok,
490 Germany), and the expression and purification of the enzyme were performed essentially as
491 described previously (Liu *et al.*, 2020). The specific activity of GGAT, AGAT, and SGAT were
492 expressed in µmoles of (Glutamate, Alanine, Serine) m^{-2} s^{-1}.
493
494 **Hydroxypyruvate reductase (HPR) activity**
495 The activity of HPR was determined in *R. stricta* and *N. tabacum* by the oxidation of
496 NADH (Tolbert *et al.*, 1970) with the following modifications. The reaction was initiated by
497 adding 4 µL of 25 Na beta-hydroxypyruvate to the reaction mix, containing 192 µL of reaction
498 buffer (100 mM K-phosphate buffer, pH 8.1, 0.15 mM NADH) and 4 µL crude extract. The
499 addition of the substrate was performed with the use of a 96-well microplate replicator. The
500 decrease in absorbance at 340 nm was monitored continuously for 5 min. To determine the
501 rate of background utilization of NADH, the controls contained 4 µL H_2O instead of the
502 substrate. The specific activity of HPR was expressed in µmoles of hydroxypyruvate m^{-2} s^{-1}.
503
504 **Glycerate kinase (GLYK) activity**
505 The activity of GK was determined by linking formation of 3-phosphoglycerate to NADH
506 oxidation using a set of coupling enzymes identical to the set of coupling enzymes used for
507 measuring rubisco activity (Walker *et al.*, 2016b). 192 µL reaction buffer (containing 50 mM
508 HEPES, pH 7.8, 10 mM $MgCl_2$, 60 mM KCl, 1 mM ATP, 0.2 mM NADH) (Kleczkowski and Randall,
509 1988) were combined with 4 µL crude protein extract, 4 µL coupling enzymes (22.5 U ml^{-1} 3-
510 phosphoglycerate kinase, 250 U mL^{-1} carbonic anhydrase, 12.5 U mL^{-1} creatine phosphokinase,
511 20 U mL^{-1} glyceraldehyde-3-phosphate dehydrogenase, 20 U mL^{-1} glycerol-3-phosphate
512 dehydrogenase, 56 U mL^{-1} triose-phosphate isomerase), and the reaction was initiated by

513 addition of 2 µL of 500 mM D-glycerate (5 mM final) (all from Sigma-Aldrich, Inc., St. Louis, MO,
514 United States); the substrate was added with the use of a 96-well microplate replicator. The
515 decrease in optical density at 340 nm was monitored for 10 min. The initial rate of reaction was
516 used to express the specific activity as µmoles glycerate m^{-2} s^{-1}.
517
518 **Data Processing and Statistical Analyses**
519 Gas exchange, stable carbon isotope, and biochemical data were visualized and analyzed using
520 custom scripts in R (R Core Team, 2021; RStudio Team, 2021). Student's t-test and repeated
521 measures Two-way ANOVA were used to measure significance ($P < 0.05$). All ANOVA tests were
522 followed with a Tukey's post-hoc test. Additionally, all gas-exchange data followed the
523 reporting format and recommendations defined in (Ely *et al.*, 2021).
524
525 ## Results
526 ***R. stricta* performs higher photorespiration than *N. tabacum* under elevated temperatures**
527 To assess the ability of *R. stricta* and *N. tabacum* to fix carbon under ambient
528 photorespiratory conditions, the temperature response of v_o, v_o/v_c, A and $A + R_L$ were measured
529 under ambient O_2 conditions (21%) at low (250 µmol PAR m^{-2} s^{-1}) and high light (1750 µmol PAR
530 m^{-2} s^{-1}) intensities (Figure 1 and Figure 2). V_o in *R. stricta* was significantly greater than *N.*
531 *tabacum* at 25°C, 30°C, 35°C, and 40°C under low light and greater at 25°C, 30°C, and 40°C at
532 high light (Figure 1A & C). At the growth temperature (~30°C), v_o in *R. stricta* was 48% (low
533 light) and 60% (high light) greater than *N. tabacum.* The relative rate of rubisco oxygenation
534 (v_o/v_c) in *R. stricta* was significantly greater than *N. tabacum* at 25°C and 40°C under low light
535 and greater at 25°C, 30°C, and 40°C under high light (Figure 1B & D). The increased v_o and v_o/v_c
536 in *R. stricta* indicate that rubisco catalyzes oxygenation reactions more frequently than *N.*
537 *tabacum* and therefore, experiences a greater photorespiratory pressure under most
538 temperatures. *R. stricta* had similar rates of *A* to *N. tabacum* at 20°C, 25°C, 35°C, and 40°C; but
539 a greater rate at 30°C under low light (Figure 2A). Under high light, *R. stricta* had similar rates of
540 *A* as compared to *N. tabacum* at 20°C, 35°C, and 40°C; but a greater rate at 25°C and 30°C
541 (Figure 2C). At the growth temperature, *A* in *R. stricta* was 20% (low light) and 16% (high light)

542 larger than *N. tabacum.* R_L, which is needed to determine gross assimilation, was greater in *R.*
543 *stricta* than *N. tabacum* at 20°C, 25°C, 30°C, 35°C, and 40°C (Supplemental Figure 1A). Gross
544 assimilation was higher in *R. stricta* than *N. tabacum* at 25°C, 30°C, and 35°C under low light
545 (Figure 2B). Under high light, gross assimilation in *R. stricta* was similar to *N. tabacum* at 20°C,
546 35°C, and 40°C; but a greater at 25°C and 30°C (Figure 2D). These results indicate that the
547 photosynthetic rate in *R. stricta* did not decrease despite high rates of photorespiration.
548
549

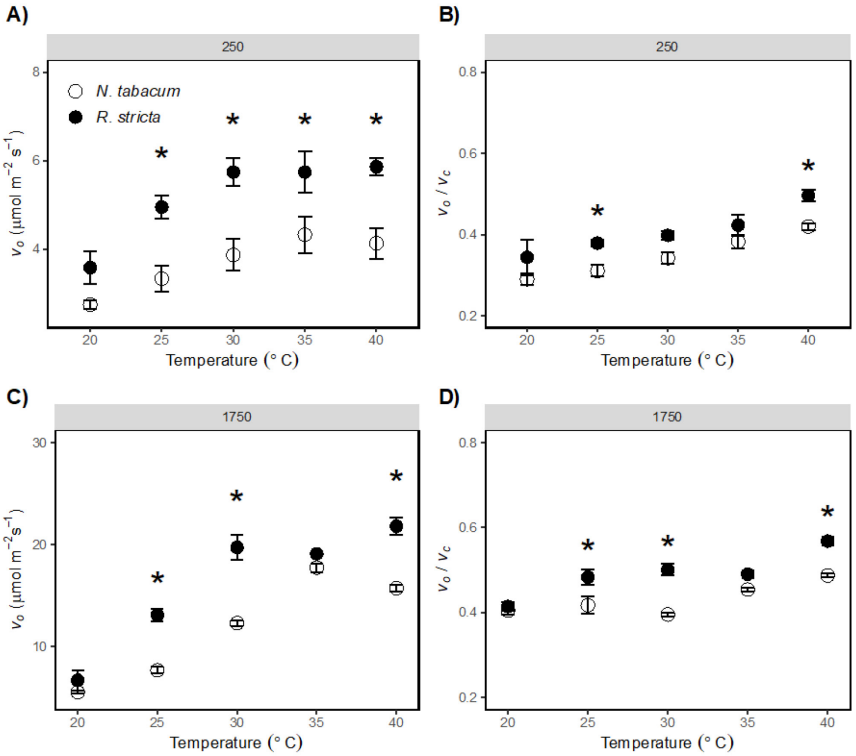

562 **Figure 1. The temperature response of rubisco oxygenation rate in *Nicotiana tabacum* and *Rhazya stricta*.** The temperature response of the oxygenation rate (v_o, A & C) and rubisco oxygenation per carboxylation (v_o/v_c, B & D) in *R. stricta* (closed symbols) and *N. tabacum* (open symbols). v_o and v_o/v_c were calculated from steady-state gas exchange measured under 40 Pa CO_2 and 250 or 1750 µmol PAR m^{-2} s^{-1}. Shown are the means of 4-5 biological replicates with ± SE bars. Significant difference between species is indicated by an asterisk as determined by Two-way ANOVA with $P < 0.05$.
567
568 To understand *R. stricta* and *N. tabacum* abilities to fix carbon under minimal
569 photorespiratory conditions, the temperature response of v_o, v_o/v_c, A, and $A + R_L$ were
570 measured under low O_2 conditions and high light (2% 1750 PAR; Supplemental Figure 2). In

571 contrast to the ambient O_2 conditions, v_o in *R. stricta* was similar to *N. tabacum* at 25°C and
572 40°C, but less than *N. tabacum* at 25°C, 30°C and 35°C (Supplemental Figure 1A). As expected,
573 the rates of v_o in both species were reduced to a fraction of the 21% values under 2% O_2. v_o/v_c
574 in *R. stricta* was similar to *N. tabacum* at 20°C, 25°C, 30°C, and 35°C, but greater than *N.*
575 *tabacum* at 40°C (Supplemental Figure 1B). Under this minimal photorespiration, *R. stricta* had
576 lower rates of A and $A + R_L$ than *N. tabacum* at 20°C, 25°C, 30°C, 35°C, and 40°C (Supplemental
577 Figure 1C and D). The results indicate under minimal photorespiratory conditions, *R. stricta*
578 ability to fix carbon is reduced compared to *N. tabacum*.
579
580
581
582
583
584
585
586
587
588
589
590
591
592
593
594

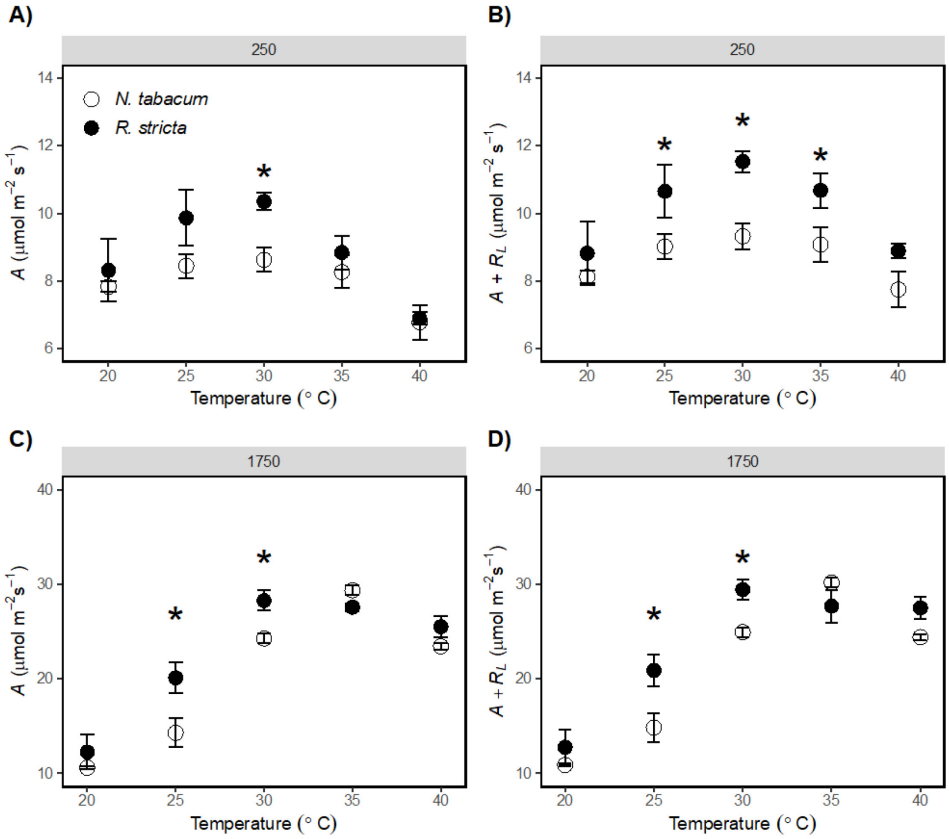

595 **Figure 2. The temperature response of net and gross assimilation rates in *Nicotiana***
596 ***tabacum* and *Rhazya stricta*.** The temperature response of net assimilation rate (A, A
597 & C) and gross assimilation rate ($A + R_L$; B & D) in *R. stricta* (closed symbols) and *N.*
598 *tabacum* (open symbols). A and $A + R_L$ were measured from steady-state gas exchange
599 at 40 Pa CO_2 and 250 or 1750 µmol PAR m^{-2} s^{-1}. Shown are the means of 4 biological
replicates with ± SE bars. Significant difference between species is indicated by an
asterisk as determined by Two-way ANOVA with $P < 0.05$.

Photosynthetic biochemical limitations of *R. stricta* and *N. tabacum*

To understand the biochemical limitations on photosynthesis, the temperature response of the J_{max} and the $v_{c,max}$ were estimated in *R. stricta* and *N. tabacum*. J_{max} in *R. stricta* was similar to *N. tabacum* at 20°C, but greater than *N. tabacum* at 25°C, 30°C, 35°C, and 40°C (Figure 3A). In contrast to J_{max}, $v_{c,max}$ did not have a consistent trend in *R. stricta*. $v_{c,max}$ in *R. stricta* was similar to *N. tabacum* at 20°C, greater than *N. tabacum* at 25°C, 30°C, and 40°C, but less than *N. tabacum* at 35°C.

To find the saturating light intensity and to understand photosynthetic capacity in *R. stricta* and *N. tabacum*, a light response curve was measured at 25°C (Supplemental Figure 3). Maximum quantum yield of CO2 fixed per photon absorbed (Φ_{CO2}) was significantly greater in *R. stricta* (0.060 ± 0.0047) than N. tabacum (0.046 ± 0.0017) at 25°C.

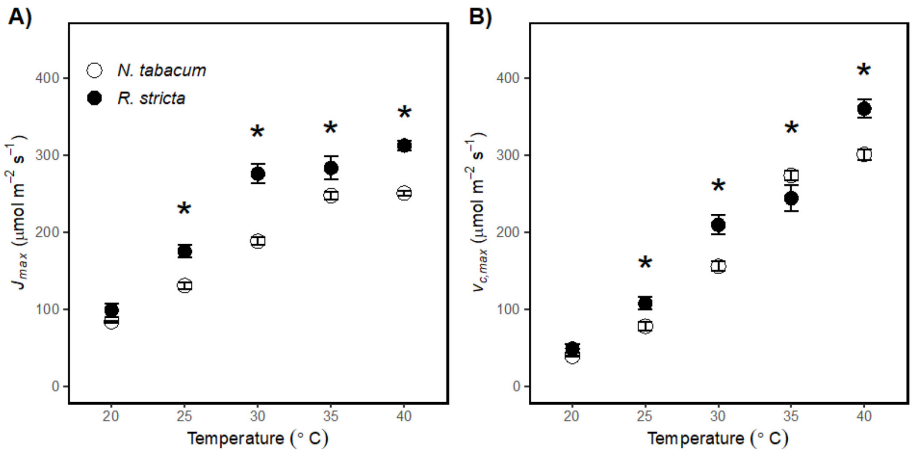

Figure 3. The temperature response of J_{max} and $v_{c,max}$ in *Nicotiana tabacum* and *Rhazya stricta*. The temperature response of the maximum rate of electron transport (J_{max}, A) and rubisco maximum carboxylation rates ($v_{c,max}$, B) in *R. stricta* (closed symbols) and *N. tabacum* (open symbols). J_{max} and $v_{c,max}$ were estimated from gas exchange measurements at 40-42 Pa CO_2 and 1750 µmol PAR m^{-2} s^{-1}. Shown are the means of 4 biological replicates with ± SE bars. Significant difference between species is indicated by an asterisk as determined by Two-way ANOVA with $P < 0.05$.

Quantifying the photorespiratory CO_2 compensation point (Γ^*) under ambient O_2 conditions links rubisco kinetics with the stoichiometry of CO_2 release per rubisco oxygenation

629 from photorespiration (Walker *et al.*, 2016a). Additionally, the temperature response of Γ^*
630 provides a key parameter needed to calculate v_o, v_c, and g_m. Γ^* in *R. stricta* was greater than *N.*
631 *tabacum* at 30°C and 40°C, but similar to *N. tabacum* at 20°C, 25°C, and 35°C (Supplemental
632 Figure 1B).
633 To understand whether differences in Γ^* are related to a variable or constant α between
634 *R. stricta* and *N. tabacum*, we measured photorespiratory discrimination (Δ_f) and the $^{12}C/^{13}C$
635 fractionation during photorespiration (f). Interestingly, there was no significant difference
636 between the species for either parameter at 25°C or 35°C (Supplemental Figure 4). To
637 understand whether oxygen sensitivity in g_m lead to misinterpretation in Δ_f and f calculation,
638 we measured at 2% and 21% oxygen at two key temperatures (25°C and 35°C) and determined
639 no oxygen sensitivity to g_m using different assumptions for photorespiratory fractionation
640 (Supplemental Figure 5).
641
642
643
644 ***Rhazya stricta* partitions CO_2 transfer conductances for increased water use efficiency**
645 The temperature response of stomatal conductance and mesophyll conductance to CO_2
646 (g_{tc} and g_m) were measured to determine the CO_2 diffusion differences between *R. stricta* and
647 *N. tabacum* (Figure 4A and C). g_{tc} was lower in *R. stricta* than *N. tabacum* at all temperatures.
648 g_m in *R. stricta* was similar to *N. tabacum* at 20°C, 25°C, and 30°C, but greater at 35°C and 40°C.
649 The results indicate that there is a tradeoff in the diffusive barriers in *R. stricta* from stomatal to
650 mesophyll conductance.

651 The temperature response of the photosynthetic limitation imposed by stomatal
652 conductance and mesophyll conductance to CO_2 (Lg_{tc} and Lg_m) were calculated to determine
653 how much g_{tc} and g_m limit photosynthetic rate (Figure 4 B and D). Lg_{tc} in *R. stricta* was greater
654 than *N. tabacum* at 35°C, but similar to *N. tabacum* at the other temperatures. Lg_m in *R. stricta*
655 was greater than *N. tabacum* at 25°C and 30°C, but similar to *N. tabacum* at the rest of the

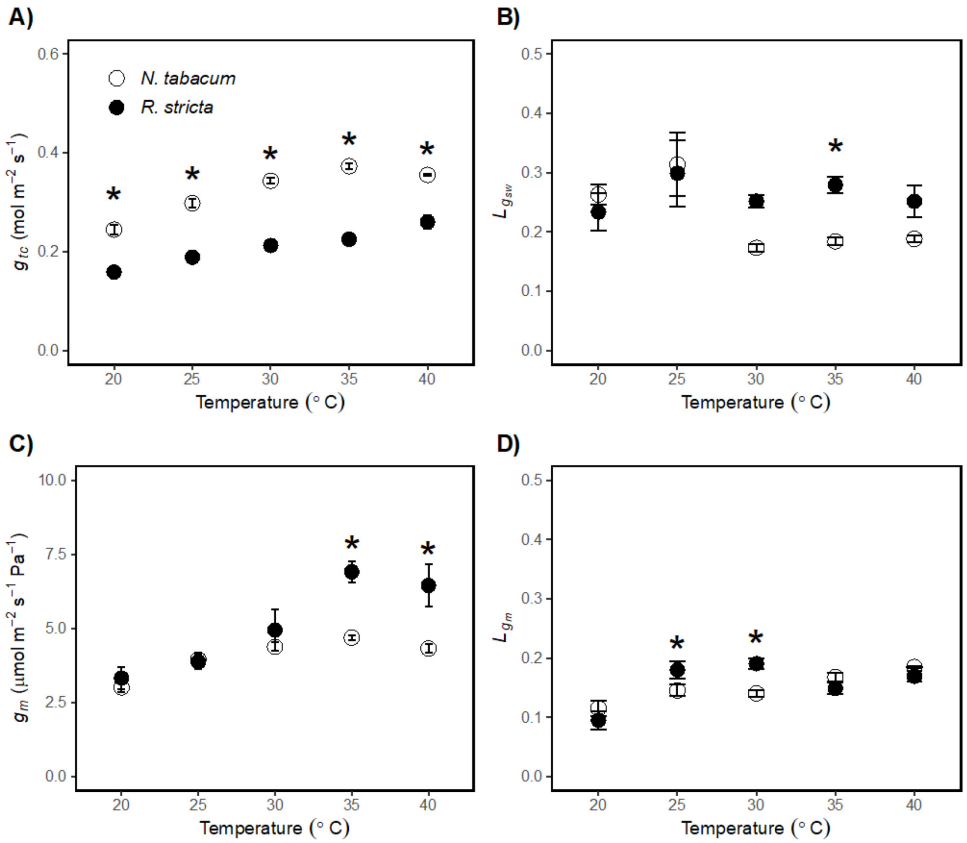

Figure 4. Temperature response of stomatal and mesophyll conductance and their limitations imposed on photosynthetic rate in *Nicotiana tabacum* and *Rhazya stricta*. The temperature response of stomatal conductance to CO_2 (g_{tc}, A), and mesophyll conductance to CO_2 (g_m, C) as well as the limitation imposed by both conductances (Lg_{tc} and Lg_m, B and D) *in R. stricta* (closed symbols) and *N. tabacum* (open symbols) . g_{tc} and g_m were measured from steady state gas exchange and on-line measurements of carbon isotope discrimination at 40 Pa CO_2 and 1750 µmol PAR m^{-2} s^{-1} (panels A & C). Lg_{tc} and Lg_m were estimated from gas exchange measurements at 40-42 Pa CO_2 and 1750 µmol PAR m^{-2} s^{-1}. Shown are the means of 4-5 biological replicates with ± SE bars. Significant difference between species is indicated by an asterisk as determined by Two-way ANOVA with $P < 0.05$.

656 temperatures. Overall, g_{tc} and g_m did not impose a significant limitation of photosynthetic rate
657 as Lg_{tc} and Lg_m did not have consistent trends across temperature for *R. stricta* or *N. tabacum*.
658 The temperature response of water use efficiency (*WUE*) was calculated to determine
659 how the CO_2 transfer conductances constrained water use in *R. stricta* and *N. tabacum*
660 (Supplemental Figure 6). *WUE* in *R. stricta* was greater compared to *N. tabacum* at 20°C, 25°C,
661 30°C, 35°C, and 40°C. The temperature response of WUE results indicate that *R. stricta* fixes
662 carbon at a lower cost of water than *N. tabacum* on a stoichiometric basis.
663
664 **Photorespiratory enzyme activity in *R. stricta* compared to *N. tabacum***
665 We measured photorespiratory enzyme activities to determine which photorespiratory
666 enzymes have higher activities and temperature responses in *R. stricta* as compared to *N.*
667 *tabacum* (Figure 5). These enzymatic activities were measured in leaves in *R. stricta* and *N.*
668 *tabacum* at 25°C and 35°C using crude protein extracts. The photorespiratory enzymes assayed
669 PGP, GO, CAT, GGAT, AGAT, SGAT, HPR, and GLYK. *R. stricta* had greater PGP and CAT activities

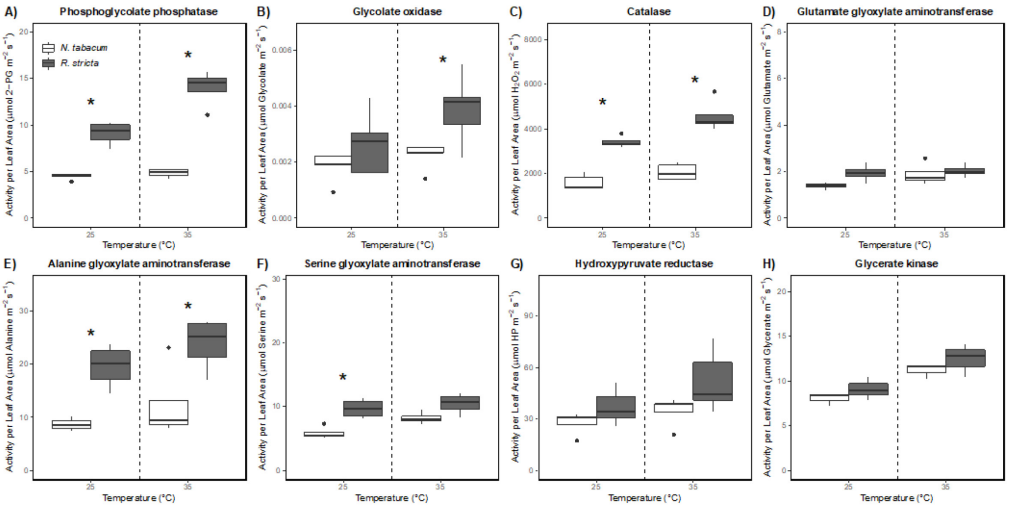

Figure 5. Photorespiratory enzymatic activities in *Nicotiana tabacum* and *Rhazya stricta* at 25°C and 35°C. Specific activities per m^2 leaf area were measured in *R. stricta* (black boxplot) and *N. tabacum* (white boxplot) using crude protein extracts for the enzymes phosphoglycolate phosphatase, glycolate oxidase, catalase, glutamate glyoxylate aminotransferase, alanine glyoxylate aminotransferase, serine glyoxylate aminotransferase, hydroxypyruvate reductase, and glycerate kinase. Shown are boxplots as well as points indicating the biological replicates. Significant difference between species is indicated by an asterisk as determined by Student's t-test with $P < 0.05$.

670 than *N. tabacum* at 25°C and 35°C. *R. stricta* had greater AGAT and SGAT activities than *N.*
671 *tabacum* at 25°C. *R. stricta* had similar GO, GGAT, HPR, and GK activities to *N. tabacum* at 25°C
672 and 35°C.

673 The temperature response ratio of the enzyme activities was calculated by dividing the
674 activity per mg protein at 35°C by the activity per mg protein at 25°C for each enzyme to
675 establish if there are greater enzyme activities (relative to 25°C) at the elevated temperature in
676 *R. stricta* and *N. tabacum* (Supplemental Figure 7). PGP had a greater relative increase in
677 activity with temperature in *R. stricta* as compared to *N. tabacum*; however, GO, CAT, GGAT,
678 AGAT, SGAT, HPR, and GLYK had similar temperature response ratios.

679

680 **Discussion**

681 ***Hallmarks of a temperature-tolerant photorespiratory pathway***

682 These results demonstrate that *R. stricta* maintains higher rates of photorespiration
683 under moderate and elevated temperatures and that these higher rates of activity correlate
684 with increased activity of key photorespiratory enzymes. The higher rates of photorespiration
685 are evident in the temperature response of v_o and v_o/v_c, which were greater in *R. stricta* than in
686 *N. tabacum* at moderate (25°C and 30°C) and elevated (35°C and 40°C) temperatures (Figure 1).
687 Higher rates of photorespiration in *R. stricta* were accompanied by increased activities of
688 specific photorespiratory enzymes. In *R. stricta*, PGP and CAT activities were greater than *N.*
689 *tabacum* at 25°C and 35°C (Figure 5A & C). These higher photorespiratory enzyme activities in
690 *R. stricta* compared to *N. tabacum* support the hypothesis that *R. stricta* has adapted to high
691 photorespiratory pressure at moderate and elevated temperature by increased activity of these
692 key enzymes. Additionally, the temperature response ratio of PGP activity in *R. stricta* was
693 larger compared to *N. tabacum* (1.55 compared to 1.07; Supplemental Figure 7). The larger
694 temperature response of PGP indicates a larger V_{max} in the *R. stricta* at elevated temperatures
695 than *N. tabacum*. The larger temperature response of PGP at elevated temperatures could not
696 be explained by gene expression differences between the species as these assays were
697 conducted *in vitro*. However, the increase could result from a more thermostable isoform of
698 PGP in *R. stricta* than *N. tabacum*.

699 Increased activity of PGP may allow photorespiration to maintain low concentrations of
700 2-PG, an inhibitor of C_3 cycle enzymes, that accumulates under moderate and elevated
701 temperatures. Past work supports the hypothesis that efficient degradation of 2-PG by PGP is
702 critical for maintaining high rates of photosynthesis under higher photorespiratory conditions.
703 For example, *Arabidopsis* overexpressing PGP maintain higher photosynthetic rates after short-
704 term and long-term exposure to elevated temperatures as compared to wild-type and maintain
705 a lower steady-state pool of 2-PG (Flügel *et al.*, 2017; Timm *et al.*, 2019). Therefore, minimizing
706 the inhibition of photosynthesis by 2-PG appears to be a key feature for increasing the
707 temperature resiliency of photorespiration in engineered and adapted plants.
708 CAT may also play a role in maintaining photosynthesis under higher photorespiratory
709 pressure by detoxifying H_2O_2. Photorespiration is a large source of H_2O_2 in the light. H_2O_2
710 functions as a signaling molecule in both stress and developmental processes, where
711 concentrations of H_2O_2 are likely under homeostatic regulation by foliar-expressed CAT in the
712 peroxisome (Dat *et al.*, 2003; Queval *et al.*, 2008; Queval *et al.*, 2007). CAT-deficient *N. tabacum*
713 has high concentrations of H_2O_2 that leads to cell death when plants were exposed to high
714 photorespiratory pressure (Dat *et al.*, 2003). Other work with CAT-deficient plants indicate the
715 enzyme is an important mediator of cellular toxicity during environmental stress (Willekens *et*
716 *al.*, 1997). Additionally, there is evidence that H_2O_2 can react with glyoxylate and/or
717 hydroxypyruvate resulting in non-enzymatic decarboxylation and release additional CO_2 from
718 photorespiration (Cousins *et al.*, 2008; Grodzinski, 1978; Halliwell *et al.*, 1974; Keech *et al.*,
719 2012; Zelitch, 1992). For example, in a mutant with reduced foliar-expressed CAT,
720 photosynthetic rates are reduced due to an increase in the stoichiometry release of CO_2 per
721 oxygenation, most likely from the non-enzymatic decarboxylation with hydroxypyruvate and
722 H_2O_2 (Bao *et al.*, 2021). This work supports the hypothesis that sufficient CAT activity plays a
723 critical role preventing elevated H_2O_2 signaling and possibly the additional loss of CO_2 from
724 photorespiration and is an adaptive strategy in *R. stricta* to moderate and elevated
725 temperatures. Interestingly, we found no evidence that *N. tabacum* actually had an increase in
726 CO_2 release per rubisco oxygenation as would be expected from excess non-enzymatic

727 decarboxylations (discussed below). This finding indicates that the role of CAT in H_2O_2 signaling
728 may be more important than any potential CO_2 loss from non-enzymatic decarboxylations.
729 Interestingly, when photorespiration was reduced under low O_2 conditions, both *A* and *A*
730 + R_L were lower in *R. stricta* compared to *N. tabacum* but were similar or slightly higher when
731 measured under ambient O_2 conditions (Supplemental Figure 2 & Figure 2). The higher rates of
732 *A* and *A* + R_L in *N. tabacum* supports that the photorespiratory pathway in *R. stricta* reduces the
733 inhibition of photosynthesis under photorespiratory conditions more efficiently than *N.*
734 *tabacum*. In other words, *A* in *N. tabacum* is more sensitive to photorespiratory intermediates,
735 despite having only half the rates of v_o. The increase in *A* and *A* + R_L under photorespiratory
736 conditions in *R. stricta* is therefore likely due to the greater activity of PGP and CAT in *R. stricta*,
737 rather than an improved ability to fix carbon. These results also indicate that photosynthesis in
738 *R. stricta* is adapted to environments with high photorespiratory pressure.
739
740 ***Managing CO_2 transfer conductance for improved water use efficiency***
741 Our results demonstrate that *R. stricta* has a higher g_m that is compensated by a lower
742 $g_{tc,}$ resulting in a similar overall CO_2 transfer conductance limitation to photosynthesis. *R. stricta*
743 exhibits a lower g_{tc} than *N. tabacum* across the entire temperature gradient (Figure 5A).
744 However, this conductance difference between *R. stricta* and *N. tabacum* does not impose a
745 larger CO_2 limitation on photosynthetic rate (Figure 5B). *R. stricta* has a greater g_m than *N.*
746 *tabacum* at elevated temperatures (Figure 5C). This difference in g_m at elevated temperatures
747 does not reduce the CO_2 limitation on photosynthetic rate (Figure 5D). So why does this re-
748 partitioning strategy exist in *R. stricta* if it does not support an increase in net CO_2 assimilation?
749 *R. stricta* appears to have re-partitioned the CO_2 transfer conductance at high temperatures
750 from the stomata, which loses water, to the mesophyll, which does not.
751 The implications of this re-partitioning of conductances result in *R. stricta* having an
752 increase in *WUE*. Although the lower g_{tc} indicates that the initial CO_2 delivery into the leaf was
753 more restricted in *R. stricta* than *N. tabacum*, it also means that water has a more restricted
754 path leaving the leaf. The lower g_{tc} in *R. stricta* resulted in a greater *WUE* than *N. tabacum*
755 (Supplemental Figure 6). The greater *WUE* indicates a lower cost of water loss per carbon

assimilated, which is an important water-saving strategy. This water-saving strategy in *R. stricta* is consistent with other stomatal conductance measurements in other C_3 desert species, but the higher g_m has not yet been described to our knowledge (Driscoll *et al.*, 2021; Driscoll *et al.*, 2020; Kannenberg *et al.*, 2021; Ogle *et al.*, 2012).

Other adaptive strategies of photosynthesis appear similar between species

Biochemical limitations of photosynthesis reveal key similarities and differences between *R. stricta* and *N. tabacum*. In *R. stricta*, the J_{max} was greater than *N. tabacum* at 25°C, 30°C, 35°C, and 40°C (Figure 3A). These higher rates of J_{max} in *R. stricta* are consistent with a higher photorespiratory capacity in *R. stricta*, since photorespiration dissipates more excitation energy from the electron transport chain than *N. tabacum* which would increase maximal rates of electron flux (Kozaki *et al.*, 1996).

In contrast to J_{max}, differences in $v_{c,max}$ were inconsistent between *R. stricta* and *N. tabacum*. In *R. stricta*, the $v_{c,max}$ was similar to N. tabacum at 20°C, and greater than *N. tabacum* at 25°C, 30°C, and 40°C (Figure 3A). Interestingly, $v_{c,max}$ in *R. stricta* was less than *N. tabacum* at 35°C. Generally, ignoring the 35°C data, there was a greater $v_{c,max}$ in *R. stricta* as temperature increased. Moreover, while we measured an increase in $v_{c,max}$ associated with temperature, others measure a $v_{c,max}$ independent of temperature in *in situ* studies of *R. stricta* (Lawson et al., 2014). Lawson *et al.,* point to a potential thermostable rubisco activase as a potential strategy *R. stricta* uses to maintain rubisco catalytic capacity and activity at elevated temperatures. Potentially, this thermotolerant rubisco activase could be the reason we see higher $v_{c,max}$ in *R. stricta* compared to *N. tabacum* at 25°C, 30°C, and 40°C. However, we did not measure rubisco activity or activation state in this study.

Carbon assimilation is in part determined by the CO_2 released from R_L. Minimizing R_L could be a strategy used by *R. stricta* to maintain a higher assimilation rate at elevated temperatures. Interestingly, R_L was greater in *R. stricta* compared to *N. tabacum* at each temperature (Supplemental Figure 1A). The higher R_L meant that *R. stricta* is respiring more non-photorespiratory CO_2 than *N. tabacum* in the light. When considering rates of carbon assimilation, *R. stricta* had higher *A* than *N. tabacum* at 30°C under low light and at 25°C and

785 30°C under high light. In contrast, when the CO_2 loss from R_L is added back, *R. stricta*
786 maintained higher $A + R_L$ than *N. tabacum* at 25°C, 30°C, and 35°C under low light, and at 25°C
787 and 30°C under high light, meaning that *R. stricta* fixed more carbon at these temperatures
788 (Figure 2). Therefore, the greater rates of R_L in *R. stricta* reduce the amount of carbon fixed and
789 does not explain why *R. stricta* can maintain higher *A* at growth temperatures (~30°C) under
790 low or high light intensity than *N. tabacum.* This result demonstrates that minimizing R_L does
791 not appear to be a strategy that *R. stricta* uses to perform photosynthesis at higher rates
792 compared to *N. tabacum* from a carbon budget perspective, but perhaps the elevated R_L
793 contributes some yet-undescribed metabolic role in the elevated temperature tolerance.
794 Photosynthetic performance can also be characterized by Γ^* which links the specificity
795 of rubisco for CO_2 over O_2 ($S_{c/o}$) to the stoichiometry of CO_2 release from rubisco oxygenation
796 from photorespiration (α). A change in Γ^* may indicate differences in $S_{c/o}$ or α and may be an
797 adaptive strategy in *R. stricta* to maintain photosynthetic performance. Interestingly, Γ^* was
798 greater at 30°C and 40°C in *R. stricta* compared to *N. tabacum*, but similar at 20°C, 25°C, and
799 35°C. When considering changes in $S_{c/o}$, past work suggest that $S_{c/o}$ varies little within higher
800 plants (Flamholz *et al.*, 2019) but *R. stricta* was not included in this analysis, therefore not ruling
801 out that it has adapted an improved $S_{c/o}$. Since the temperature response of Γ^* does not show
802 any decrease in *R. stricta* as compared to *N. tabacum,* we do not see any evidence for adaptive
803 changes in $S_{c/o}$ as a strategy that *R. stricta* uses to perform photosynthesis.
804 When considering α, previous work has resolved α to be 0.5 moles of CO_2 loss per
805 rubisco oxygenation. The CO_2 loss is primarily attributed to the decarboxylation of glycine from
806 the mitochondrion; however, if additional CO_2 is lost from NED in the peroxisome, the
807 additional moles of CO_2 loss would be captured in this term. Determining α *in vivo* is difficult
808 since it is integral to many of the simplifications and assumptions needed to interpret any gas
809 exchange data in C_3 plants. For example, taken at face value, the Γ^* data would suggest that α
810 actually increases in *R. stricta* as compared to *N. tabacum* which, if true, would mean that *R.*
811 *stricta* has a less efficient photorespiratory pathway from a carbon balance perspective
812 assuming a similar $S_{c/o}$. However, determining Γ^* requires assumptions of α to calculate Γ^* in
813 the first place (i.e., g_m) clouding this interpretation. As an independent indicator to support the

814 use of a constant α in all our calculations, we surmised that additional CO_2 release would carry
815 a different isotopic fractionation since it would arise from a different reaction (not glycine
816 decarboxylase). This is supported by past work indicating that the transgenic rice with reduced
817 glycine decarboxylase activity (and more alternative decarboxylation reactions with a higher α)
818 have greatly decreased *f* values from 16.2‰ to ~3.3‰ (Giuliani *et al.*, 2019).
819 To determine if there was a decreased (or even different) *f* value consistent with a
820 change in α, we measured Δ_f and *f* in *R. stricta* and *N. tabacum*. Interestingly, there was no
821 significant difference between the species for either parameter at 25°C or 35°C (Supplemental
822 Figure 4). Therefore, we do not see any evidence for differences in the reactions contributing to
823 α between *R. stricta* and *N. tabacum*. Interestingly, there was an increase in R_L in *R. stricta*
824 relative to *N. tabacum* but this can't be a reflection of a different α since this rate was not
825 sensitive to different rates of photorespiration as indicated by the common intercept of the CO_2
826 response curves measured under different illumination during the common-intersection
827 measurements. This approach cannot preclude a small rate of non-enzymatic decarboxylations
828 or a reaction that has the same fractionation as glycine decarboxylation, but for the purposes of
829 this study, we assume that α = 0.5 for all the gas-exchange calculations. This assumption also
830 suggests that the protection against these reactions by increased catalase expression may be
831 accompanied by a self-regulating mechanism to down-regulate rubisco activity when catalase
832 activity is too low to prevent them from happening, explaining why higher activities of catalase
833 are important in *R. stricta*, but non-enzymatic decarboxylations do not appear to occur at high
834 rates in *N. tabacum*.
835 Although *R. stricta* and *N. tabacum* share the same photosynthetic pathway (C_3 cycle),
836 differences in Φ_{CO2} reveal changes in photosynthetic capacity (Supplemental Figure 3). At 25°C,
837 *R. stricta* had a significantly greater Φ_{CO2} (0.060 ± 0.0047) than *N. tabacum* (0.046 ± 0.0017).
838 The question arises: What occurs between light absorption by the antennae and the
839 carboxylation of CO_2 by rubisco that allows *R. stricta* to maximize the number of CO_2 fixed per
840 photon absorbed? Perhaps non-photochemical quenching and/or photosynthetic control
841 through cytochrome b_6f is less, leading to a higher light use efficiency of photosystem II and
842 higher electron transfer rates per photon absorbed (Eberhard *et al.*, 2008). However, at low

843 light absorption, we do not expect substantial non-photochemical quenching to occur in either
844 species (Strand *et al.*, 2023). To understand the differences in coupling between the light
845 absorption and Φ_{CO2}, we would need more characterizations of the upstream light reactions in
846 both species.
847
848 ***Concluding Remarks***
849 These results suggest important adaptive strategies used by *R. stricta* to maintain
850 photosynthetic rates under moderate and elevated temperatures. To maintain high rates of
851 photorespiration under most temperatures with minimal inhibitor accumulation, *R. stricta*
852 increases photorespiratory capacity by reducing enzymatic bottlenecks. A second adaptive
853 strategy in *R. stricta* to elevated temperatures is to increase water-use efficiency by lowering g_{tc}
854 and increasing g_m. These strategies found in *R. stricta* may inform breeding and engineering
855 efforts in other C_3 species to improve photosynthetic efficiency at elevated temperature.
856
857
858 **Acknowledgement**
859 We would like to thank Dr. Salman Gulzar for help with *R. stric*ta cultivation and
860 ecophysiology. We additionally thank Audrey Johnson for the valuable work and discussion
861 during the cultivation process of *R. stricta*. We thank Deserah Strand for helpful discussion
862 regarding Φ_{CO2} and potential adaptations in the light reaction pathway. We also thank Jim Klug
863 and Cody Keilen (MSU Growth Chamber Facility) for overall greenhouse maintenance and pest
864 management during plant cultivation. Finally, we would like to thank Hilary Stewart Williams for
865 help setting up the tunable diode laser measurement system, including the software and
866 hardware.
867
868
869
870
871
872
873
874
875

Literature Cited

Uncategorized References

Abadie, C., Boex-Fontvieille, E. R., Carroll, A. J., & Tcherkez, G. (2016). In vivo stoichiometry of photorespiratory metabolism. *Nature Plants, 2*(2), 1-4.

Aebi, H. E. (1983). Catalase. In: Bergmeyer, H.U., Ed., Methods of Enzymatic Analysis. *Verlag Chemie, Weinheim*, 273-286.

Anderson, L. E. (1971). Chloroplast and cytoplasmic enzymes II. Pea leaf triose phosphate isomerases. *Biochimica et Biophysica Acta (BBA) - Enzymology, 235*(1), 237-244. doi:https://doi.org/10.1016/0005-2744(71)90051-9

Baker, A. L., & Tolbert, N. E. (1966). Glycolate oxidase (ferredoxin containing form). Methods in Enzymology. *Academic Press, 9*, 339-342.

Bao, H., Morency, M., Rianti, W., Saeheng, S., Roje, S., Weber, A. P. M., & Walker, B. J. (2021). Catalase protects against nonenzymatic decarboxylations during photorespiration in Arabidopsis thaliana. *Plant Direct, 5*(12), e366. doi:https://doi.org/10.1002/pld3.366

Barbour, M. M., McDowell, N. G., Tcherkez, G., Bickford, C. P., & Hanson, D. T. (2007). A new measurement technique reveals rapid post-illumination changes in the carbon isotope composition of leaf-respired CO2. *Plant, Cell & Environment, 30*(4), 469-482. doi:https://doi.org/10.1111/j.1365-3040.2007.01634.x

Bauwe, H., Hagemann, M., Kern, R., & Timm, S. (2012). Photorespiration has a dual origin and manifold links to central metabolism. *Current Opinion in Plant Biology, 15*(3), 269-275. doi:10.1016/j.pbi.2012.01.008

Cousins, A. B., Pracharoenwattana, I., Zhou, W., Smith, S. M., & Badger, M. R. (2008). Peroxisomal malate dehydrogenase is not essential for photorespiration in Arabidopsis but its absence causes an increase in the stoichiometry of photorespiratory CO2 release. *Plant Physiology, 148*(2), 786-795. doi:10.1104/pp.108.122622

Dat, J. F., Pellinen, R., Beeckman, T., Van De Cotte, B., Langebartels, C., Kangasjärvi, J., . . . Van Breusegem, F. (2003). Changes in hydrogen peroxide homeostasis trigger an active cell death process in tobacco. *The Plant Journal, 33*(4), 621-632. doi:https://doi.org/10.1046/j.1365-313X.2003.01655.x

De Souza, A. P., Burgess, S. J., Doran, L., Hansen, J., Manukyan, L., Maryn, N., . . . Long, S. P. (2022). Soybean photosynthesis and crop yield are improved by accelerating recovery from photoprotection. *Science, 377*(6608), 851-854. doi:doi:10.1126/science.adc9831

Driscoll, A. W., Bitter, N. Q., & Ehleringer, J. R. (2021). Interactions among intrinsic water-use efficiency and climate influence growth and flowering in a common desert shrub. *Oecologia, 197*(4), 1027-1038. doi:10.1007/s00442-020-04825-3

Driscoll, A. W., Bitter, N. Q., Sandquist, D. R., & Ehleringer, J. R. (2020). Multidecadal records of intrinsic water-use efficiency in the desert shrub Encelia farinosa reveal strong responses to climate change. *Proceedings of the National Academy of Sciences, 117*(31), 18161-18168. doi:doi:10.1073/pnas.2008345117

Eberhard, S., Finazzi, G., & Wollman, F. A. (2008). The dynamics of photosynthesis. *Annu Rev Genet, 42*, 463-515. doi:10.1146/annurev.genet.42.110807.091452

Ely, K. S., Rogers, A., Agarwal, D. A., Ainsworth, E. A., Albert, L. P., Ali, A., . . . Yang, D. (2021). A reporting format for leaf-level gas exchange data and metadata. *Ecological Informatics, 61*, 101232. doi:https://doi.org/10.1016/j.ecoinf.2021.101232

Evans, J. R., Sharkey, T. D., Berry, J. A., & Farquhar, G. D. (1986). Carbon Isotope Discrimination measured Concurrently with Gas Exchange to Investigate CO2 Diffusion in Leaves of Higher Plants. *Functional Plant Biology, 13*(2), 281-292. doi:https://doi.org/10.1071/PP9860281

Evans, J. R., & von Caemmerer, S. (2013). Temperature response of carbon isotope discrimination and mesophyll conductance in tobacco. *Plant Cell Environ, 36*(4), 745-756. doi:10.1111/j.1365-3040.2012.02591.x

Farquhar, G., O'Leary, M., & Berry, J. (1982). On the Relationship Between Carbon Isotope Discrimination and the Intercellular Carbon Dioxide Concentration in Leaves. *Functional Plant Biology, 9*(2), 121-137. doi:https://doi.org/10.1071/PP9820121

Farquhar, G. D., & Cernusak, L. A. (2012). Ternary effects on the gas exchange of isotopologues of carbon dioxide. *Plant, Cell & Environment, 35*(7), 1221-1231. doi:https://doi.org/10.1111/j.1365-3040.2012.02484.x

Flamholz, A. I., Prywes, N., Moran, U., Davidi, D., Bar-On, Y. M., Oltrogge, L. M., . . . Milo, R. (2019). Revisiting Trade-offs between Rubisco Kinetic Parameters. *Biochemistry, 58*(31), 3365-3376. doi:10.1021/acs.biochem.9b00237

Flügel, F., Timm, S., Arrivault, S., Florian, A., Stitt, M., Fernie, A. R., & Bauwe, H. (2017). The Photorespiratory Metabolite 2-Phosphoglycolate Regulates Photosynthesis and Starch Accumulation in Arabidopsis. *The Plant Cell, 29*(10), 2537-2551. doi:10.1105/tpc.17.00256

Fu, X., Gregory, L. M., Weise, S. E., & Walker, B. J. (2023). Integrated flux and pool size analysis in plant central metabolism reveals unique roles of glycine and serine during photorespiration. *Nature Plants, 9*(1), 169-178. doi:10.1038/s41477-022-01294-9

Giuliani, R., Karki, S., Covshoff, S., Lin, H.-C., Coe, R. A., Koteyeva, N. K., . . . Cousins, A. B. (2019). Knockdown of glycine decarboxylase complex alters photorespiratory carbon isotope fractionation in Oryza sativa leaves. *Journal of Experimental Botany, 70*(10), 2773-2786. doi:10.1093/jxb/erz083

Gregory, L. M., McClain, A. M., Kramer, D. M., Pardo, J. D., Smith, K. E., Tessmer, O. L., . . . Sharkey, T. D. (2021). The triose phosphate utilization limitation of photosynthetic rate: Out of global models but important for leaf models. *Plant Cell Environ, 44*(10), 3223-3226. doi:10.1111/pce.14153

Grodzinski, B. (1978). Glyoxylate decarboxylation during photorespiration. *Planta, 144*(1), 31-37. doi:10.1007/BF00385004

Hall, N. P., & Keys, A. J. (1983). Temperature dependence of the enzymic carboxylation and oxygenation of ribulose 1, 5-bisphosphate in relation to effects of temperature on photosynthesis. *Plant Physiology, 72*(4), 945-948.

Halliwell, B., & Butt, V. S. (1974). Oxidative decarboxylation of glycollate and glyoxylate by leaf peroxisomes. *The Biochemical journal, 138*(2), 217-224. doi:10.1042/bj1380217

Heinze, M., & Gerhardt, B. (2002). Plant Catalases. In A. Baker & I. A. Graham (Eds.), *Plant Peroxisomes: Biochemistry, Cell Biology and Biotechnological Applications* (pp. 103-140). Dordrecht: Springer Netherlands.

Hermida-Carrera, C., Kapralov, M. V., & Galmés, J. (2016). Rubisco Catalytic Properties and Temperature Response in Crops. *Plant Physiology, 171*(4), 2549-2561. doi:10.1104/pp.16.01846

Jordan, D. B., & Ogren, W. L. (1984). The CO2/O2 specificity of ribulose 1,5-bisphosphate carboxylase/oxygenase. *Planta, 161*(4), 308-313. doi:10.1007/BF00398720

Kannenberg, S. A., Driscoll, A. W., Szejner, P., Anderegg, W. R. L., & Ehleringer, J. R. (2021). Rapid increases in shrubland and forest intrinsic water-use efficiency during an ongoing megadrought. *Proceedings of the National Academy of Sciences, 118*(52), e2118052118. doi:doi:10.1073/pnas.2118052118

Keech, O., Zhou, W., Fenske, R., Colas-des-Francs-Small, C., Bussell, J. D., Badger, M. R., & Smith, S. M. (2012). The Genetic Dissection of a Short-Term Response to Low CO₂ Supports the Possibility for Peroxide-Mediated Decarboxylation of Photorespiratory Intermediates in the Peroxisome. *Molecular Plant, 5*(6), 1413-1416. doi:10.1093/mp/sss104

Kendziorek, M., & Paszkowski, A. (2008). Properties of serine:glyoxylate aminotransferase purified from Arabidopsis thaliana leaves. *Acta Biochimica et Biophysica Sinica, 40*(2), 102-110. doi:10.1111/j.1745-7270.2008.00383.x

Kozaki, A., & Takeba, G. (1996). Photorespiration protects C3 plants from photooxidation. *Nature, 384*(6609), 557-560. doi:10.1038/384557a0

Kromdijk, J., Głowacka, K., Leonelli, L., Gabilly, S. T., Iwai, M., Niyogi, K. K., & Long, S. P. (2016). Improving photosynthesis and crop productivity by accelerating recovery from photoprotection. *Science, 354*(6314), 857-861. doi:doi:10.1126/science.aai8878

Laisk, A. K. (1977). Kinetics of photosynthesis and photorespiration of C3 in plants.

Larkindale, J., & Huang, B. (2004). Changes of lipid composition and saturation level in leaves and roots for heat-stressed and heat-acclimated creeping bentgrass (Agrostis stolonifera). *Environmental and Experimental Botany, 51*(1), 57-67. doi:https://doi.org/10.1016/S0098-8472(03)00060-1

Lawrence, M. G. (2005). The Relationship between Relative Humidity and the Dewpoint Temperature in Moist Air: A Simple Conversion and Applications. *Bulletin of the American Meteorological Society, 86*(2), 225-234. doi:10.1175/bams-86-2-225

Lawson, T., Davey, P. A., Yates, S. A., Bechtold, U., Baeshen, M., Baeshen, N., . . . Mullineaux, P. M. (2014). C3 photosynthesis in the desert plant Rhazya stricta is fully functional at high temperatures and light intensities. *New Phytologist, 201*(3), 862-873. doi:https://doi.org/10.1111/nph.12559

Liepman, A. H., & Olsen, L. J. (2001). Peroxisomal alanine : glyoxylate aminotransferase (AGT1) is a photorespiratory enzyme with multiple substrates in Arabidopsis thaliana. *The Plant Journal, 25*(5), 487-498. doi:https://doi.org/10.1046/j.1365-313x.2001.00961.x

Liepman, A. H., & Olsen, L. J. (2003). Alanine Aminotransferase Homologs Catalyze the Glutamate:Glyoxylate Aminotransferase Reaction in Peroxisomes of Arabidopsis. *Plant Physiology, 131*(1), 215-227. doi:10.1104/pp.011460

Liu, L., Zhong, S., Yang, R., Hu, H., Yu, D., Zhu, D., . . . Gong, D. (2008). Expression, purification, and initial characterization of human alanine aminotransferase (ALT) isoenzyme 1 and 2

in High-five insect cells. *Protein Expression and Purification, 60*(2), 225-231. doi:https://doi.org/10.1016/j.pep.2008.04.006

Liu, Y., Guérard, F., Hodges, M., & Jossier, M. (2020). Phosphomimetic T335D Mutation of Hydroxypyruvate Reductase 1 Modifies Cofactor Specificity and Impacts Arabidopsis Growth in Air1. *Plant Physiology, 183*(1), 194-205. doi:10.1104/pp.19.01225

Marcum, K. B. (1998). Cell Membrane Thermostability and Whole-Plant Heat Tolerance of Kentucky Bluegrass. *Crop Science, 38*(5), cropsci1998.0011183X003800050017x. doi:https://doi.org/10.2135/cropsci1998.0011183X003800050017x

McClain, A. M., & Sharkey, T. D. (2023). Rapid CO2 changes cause oscillations in photosynthesis that implicate PSI acceptor-side limitations. *Journal of Experimental Botany*. doi:10.1093/jxb/erad084

Moore, C. E., Meacham-Hensold, K., Lemonnier, P., Slattery, R. A., Benjamin, C., Bernacchi, C. J., . . . Cavanagh, A. P. (2021). The effect of increasing temperature on crop photosynthesis: from enzymes to ecosystems. *Journal of Experimental Botany, 72*(8), 2822-2844. doi:10.1093/jxb/erab090

Ogle, K., Lucas, R. W., Bentley, L. P., Cable, J. M., Barron-Gafford, G. A., Griffith, A., . . . Tissue, D. T. (2012). Differential daytime and night-time stomatal behavior in plants from North American deserts. *New Phytologist, 194*(2), 464-476. doi:https://doi.org/10.1111/j.1469-8137.2012.04068.x

Pai, S.-C., Yang, C.-C., & Riley, J. P. (1990). Effects of acidity and molybdate concentration on the kinetics of the formation of the phosphoantimonylmolybdenum blue complex. *Analytica Chimica Acta, 229*, 115-120.

Pörtner, H. O., Roberts, D. C., Tignor, M., Poloczanska, E. S., Mintenbeck, K., Alegría, A., . . . (eds.). (2022). IPCC, 2022: Climate Change 2022: Impacts, Adaptation, and Vulnerability. *Cambridge Univeristy Press*.

Prasertthai, P., Paethaisong, W., Theerakulpisut, P., & Dongsansuk, A. (2022). High Temperature Alters Leaf Lipid Membrane Composition Associated with Photochemistry of PSII and Membrane Thermostability in Rice Seedlings. *Plants (Basel), 11*(11). doi:10.3390/plants11111454

Queval, G., Hager, J., Gakière, B., & Noctor, G. (2008). Why are literature data for H2O2 contents so variable? A discussion of potential difficulties in the quantitative assay of leaf extracts. *Journal of Experimental Botany, 59*(2), 135-146. doi:10.1093/jxb/erm193

Queval, G., Issakidis-Bourguet, E., Hoeberichts, F. A., Vandorpe, M., Gakière, B., Vanacker, H., . . . Noctor, G. (2007). Conditional oxidative stress responses in the Arabidopsis photorespiratory mutant cat2 demonstrate that redox state is a key modulator of daylength-dependent gene expression, and define photoperiod as a crucial factor in the regulation of H2O2-induced cell death. *The Plant Journal, 52*(4), 640-657. doi:https://doi.org/10.1111/j.1365-313X.2007.03263.x

R Core Team. (2021). R: A Language and Environment for Statistical Computing. Vienna, Austria: R Foundation for Statistical Computing. Retrieved from https://www.R-project.org

Rawson, H. M., Begg, J. E., & Woodward, R. G. (1977). The effect of atmospheric humidity on photosynthesis, transpiration and water use efficiency of leaves of several plant species. *Planta, 134*(1), 5-10. doi:10.1007/BF00390086

RStudio Team. (2021). RStudio: Integrated Development Environment for R. Boston, MA: RStudio, PBC. Retrieved from http://www.rstudio.com/

Saathoff, A. J., & Welles, J. (2021). Gas exchange measurements in the unsteady state. *Plant, Cell & Environment, 44*(11), 3509-3523. doi:https://doi.org/10.1111/pce.14178

Schwarte, S., & Bauwe, H. (2007). Identification of the Photorespiratory 2-Phosphoglycolate Phosphatase, PGLP1, in Arabidopsis. *Plant Physiology, 144*(3), 1580-1586. doi:10.1104/pp.107.099192

Shen, J., Zeng, Y., Zhuang, X., Sun, L., Yao, X., Pimpl, P., & Jiang, L. (2013). Organelle pH in the Arabidopsis Endomembrane System. *Molecular Plant, 6*(5), 1419-1437. doi:https://doi.org/10.1093/mp/sst079

Somerville, C. R. (2001). An early Arabidopsis demonstration. Resolving a few issues concerning photorespiration. *Plant Physiology, 125*(1), 20-24.

Somerville, C. R., & Ogren, W. L. (1980). Photorespiration mutants of Arabidopsis thaliana deficient in serine-glyoxylate aminotransferase activity. *Proceedings of the National Academy of Sciences, 77*(5), 2684-2687.

South, P. F., Cavanagh, A. P., Lopez-Calcagno, P. E., Raines, C. A., & Ort, D. R. (2018). Optimizing photorespiration for improved crop productivity. *Journal of Integrative Plant Biology, 60*(12), 1217-1230. doi:https://doi.org/10.1111/jipb.12709

Stinziano, J. R., Morgan, P. B., Lynch, D. J., Saathoff, A. J., McDermitt, D. K., & Hanson, D. T. (2017). The rapid A–Ci response: photosynthesis in the phenomic era. *Plant, Cell & Environment, 40*(8), 1256-1262. doi:https://doi.org/10.1111/pce.12911

Strand, D. D., Karcher, D., Ruf, S., Schadach, A., Schöttler, M. A., Sandoval-Ibañez, O., . . . Bock, R. (2023). Characterization of mutants deficient in N-terminal phosphorylation of the chloroplast ATP synthase subunit β. *Plant Physiol, 191*(3), 1818-1835. doi:10.1093/plphys/kiad013

Tazoe, Y., von Caemmerer, S., Estavillo, G. M., & Evans, J. R. (2011). Using tunable diode laser spectroscopy to measure carbon isotope discrimination and mesophyll conductance to CO2 diffusion dynamically at different CO2 concentrations. *Plant, Cell & Environment, 34*(4), 580-591. doi:https://doi.org/10.1111/j.1365-3040.2010.02264.x

Tcherkez, G. (2006). How large is the carbon isotope fractionation of the photorespiratory enzyme glycine decarboxylase? *Functional Plant Biology, 33*(10), 911-920. doi:https://doi.org/10.1071/FP06098

Timm, S., Woitschach, F., Heise, C., Hagemann, M., & Bauwe, H. (2019). Faster removal of 2-phosphoglycolate through photorespiration improves abiotic stress tolerance of arabidopsis. *Plants, 8*(12). doi:10.3390/plants8120563

Tolbert, N. E., Yamazaki, R. K., & Oeser, A. (1970). Localization and Properties of Hydroxypyruvate and Glyoxylate Reductases in Spinach Leaf Particles. *Journal of Biological Chemistry, 245*(19), 5129-5136. doi:https://doi.org/10.1016/S0021-9258(18)62827-3

Ubierna, N., Holloway-Phillips, M.-M., & Farquhar, G. D. (2018). Using Stable Carbon Isotopes to Study C3 and C4 Photosynthesis: Models and Calculations. In S. Covshoff (Ed.), *Photosynthesis: Methods and Protocols* (pp. 155-196). New York, NY: Springer New York.

Urban, J., Ingwers, M., McGuire, M. A., & Teskey, R. O. (2017a). Stomatal conductance increases with rising temperature. *Plant Signal Behav, 12*(8), e1356534. doi:10.1080/15592324.2017.1356534

Urban, J., Ingwers, M. W., McGuire, M. A., & Teskey, R. O. (2017b). Increase in leaf temperature opens stomata and decouples net photosynthesis from stomatal conductance in Pinus taeda and Populus deltoides x nigra. *J Exp Bot, 68*(7), 1757-1767. doi:10.1093/jxb/erx052

Vialet-Chabrand, S., Matthews, J. S. A., Brendel, O., Blatt, M. R., Wang, Y., Hills, A., . . . Lawson, T. (2016). Modelling water use efficiency in a dynamic environment: An example using Arabidopsis thaliana. *Plant Science, 251*, 65-74. doi:https://doi.org/10.1016/j.plantsci.2016.06.016

Von Caemmerer, S. (2000). *Biochemical models of leaf photosynthesis*: Csiro publishing.

von Caemmerer, S., & Evans, J. R. (2015). Temperature responses of mesophyll conductance differ greatly between species. *Plant, Cell & Environment, 38*(4), 629-637. doi:https://doi.org/10.1111/pce.12449

Walker, B. J., & Cousins, A. B. (2013). Influence of temperature on measurements of the CO2 compensation point: differences between the Laisk and O2-exchange methods. *J Exp Bot, 64*(7), 1893-1905. doi:10.1093/jxb/ert058

Walker, B. J., Kramer, D. M., Fisher, N., & Fu, X. (2020). Flexibility in the Energy Balancing Network of Photosynthesis Enables Safe Operation under Changing Environmental Conditions. *Plants, 9*(3), 301. Retrieved from https://www.mdpi.com/2223-7747/9/3/301

Walker, B. J., Skabelund, D. C., Busch, F. A., & Ort, D. R. (2016a). An improved approach for measuring the impact of multiple CO2 conductances on the apparent photorespiratory CO2 compensation point through slope–intercept regression. *Plant, Cell & Environment, 39*(6), 1198-1203. doi:https://doi.org/10.1111/pce.12722

Walker, B. J., South, P. F., & Ort, D. R. (2016b). Physiological evidence for plasticity in glycolate/glycerate transport during photorespiration. *Photosynthesis Research, 129*(1), 93-103. doi:10.1007/s11120-016-0277-3

Warren, C. R. (2004). The photosynthetic limitation posed by internal conductance to CO2 movement is increased by nutrient supply. *Journal of Experimental Botany, 55*(406), 2313-2321. doi:10.1093/jxb/erh239

Willekens, H., Chamnongpol, S., Davey, M., Schraudner, M., Langebartels, C., Van Montagu, M., . . . Van Camp, W. (1997). Catalase is a sink for H2O2 and is indispensable for stress defence in C3 plants. *The EMBO Journal, 16*(16), 4806-4816. doi:https://doi.org/10.1093/emboj/16.16.4806

Zelitch, I. (1989). Selection and Characterization of Tobacco Plants with Novel O2-Resistant Photosynthesis. *Plant Physiology, 90*(4), 1457-1464. doi:10.1104/pp.90.4.1457

Zelitch, I. (1992). Factors Affecting Expression of Enhanced Catalase Activity in a Tobacco Mutant with O2-Resistant Photosynthesis. *Plant Physiology, 98*(4), 1330-1335. doi:10.1104/pp.98.4.1330

Zelitch, I., Schultes, N. P., Peterson, R. B., Brown, P., & Brutnell, T. P. (2008). High Glycolate Oxidase Activity Is Required for Survival of Maize in Normal Air *Plant Physiology, 149*(1), 195-204. doi:10.1104/pp.108.128439

1134